

Simulation of Co-precipitation Kinetics of γ' and γ'' in Superalloy 718



Fan Zhang, Weisheng Cao, Chuan Zhang, Shuanglin Chen, Jun Zhu and Duchao Lv

Abstract In this paper, we will study the co-precipitation kinetics of phases in Superalloy 718 using the simulation tool we have developed using the CALPHAD approach. This tool considers concurrent nucleation, growth and coarsening of these precipitates. Furthermore, it is directly integrated with thermodynamic calculation engine to obtain instant update of phase information, such as the composition of the matrix and the nucleation driving force for each precipitate. In addition to the average particle size, the more advanced KWN (Kampmann and Wagner Numerical) model was implemented to allow for predication of the full evolution of the particle size distribution (PSD). In this paper, we will perform virtual experiments using this tool to simulate the co-precipitation of the γ' and γ'' phases under different heat treatment conditions. Simulation results, such as temporal evolution of volume fraction, number density, and mean size of the precipitates, as well as the final particle size distribution will be presented and discussed. The impact of δ precipitate and the initial microstructure will also be briefly discussed. These virtual experimental results can be used to understand the microstructural features of Superalloy 718 and serve as guidance for further optimization of heat treatment schedule.

F. Zhang (✉) · W. Cao · C. Zhang · S. Chen · J. Zhu · D. Lv
CompuTherm LLC, 8401, Greenway Blvd, Middleton WI53562, USA
e-mail: fan.zhang@computherm.com

W. Cao
e-mail: weisheng.cao@computherm.com

C. Zhang
e-mail: chuan.zhang@computherm.com

S. Chen
e-mail: shuanglin.chen@computherm.com

J. Zhu
e-mail: junzhu@computherm.com

D. Lv
e-mail: duchao.lv@computherm.com

Keywords CALPHAD approach • Alloy 718 • High-throughput calculation
Thermodynamic calculation • Precipitation simulation

Introduction

Alloy 718 is a prominent superalloy that has been used in the aerospace industry for more than 50 years. The strengthening mechanism of Superalloy 718 is unique due to the co-precipitation of ordered body center tetragonal DO_{22} γ'' and ordered L1_2 γ' in the FCC γ matrix. In addition to these two precipitate phases, the δ phase with orthorhombic crystal structure tends to precipitate and coarsen when the component parts are exposed to high temperature for long time, and is usually detrimental to the alloy properties. Since all these three precipitates consume similar alloying elements, the final microstructure is the result of competition/co-precipitation of these three phases. Although plenty of processing/property relationship data have been published, systematic data on the co-precipitation kinetics of these phases during heat treatment are very limited. The purpose of this study is to understand the effect of various heat treatment conditions on the co-precipitation of the γ' and γ'' phases using a simulation approach.

Precipitation is a complex process involving the simultaneous occurrence of nucleation, growth and coarsening. Accurate modeling of the precipitation process requires a synchronous consideration of all these contributions to simulate the temporal evolution of microstructure and the corresponding responses of mechanical properties. Moreover, the phase equilibrium information as well as the composition and mobility data of the matrix phase need to be constantly updated as the nucleation, growth and coarsening proceed. Therefore, precipitation simulation needs to be directly coupled with thermodynamic calculation. The modeling tool used in this work was developed using the CALPHAD approach [1, 2]. The original motivation of the CALPHAD approach is for calculating multi-component and multi-phase diagrams. The theoretical basis of phase diagram calculation rests on the fact that the location of a phase boundary is the result of stability competition between two or more phases. The essence of this approach is to develop thermodynamic databases of multi-component systems using the available experimental data of lower order systems, i.e., binaries and ternaries. In recent years, the CALPHAD approach has been used to develop mobility databases of multi-component systems, and the combined thermodynamic database and mobility database provide model parameters for the calculation of phase equilibrium between the matrix and the precipitate phases, the nucleation driving force of precipitates, and diffusion coefficients necessary for the precipitation simulation.

In this work, the modeling tool developed at CompuTherm is used to simulate the precipitation kinetics of multi-component Alloy 718. The modeling tool includes both software and thermodynamic/mobility databases. The precipitation module is seamlessly integrated with thermodynamic calculation engine to obtain instant update information of the matrix phase and precipitate phases. The kinetic

simulation employs models to treat the concomitant events: nucleation, growth/dissolution and coarsening. The nucleation is described on the basis of the classical nucleation theory. In this module, the multi-component growth model is modified on the basis of that proposed by Morral and Purdy [3], so that it is able to treat the growth/dissolution of various precipitate phases. The coarsening model characterizes the curvature-driven particle growth, and is based on the LSW theory [4, 5]. A more advanced KWN (Kampmann and Wagner Numerical) model [6] is implemented for the prediction of the full evolution of the particle size distribution (PSD) in addition to average quantities. The obtained microstructure information (e.g., volume fraction, number density, mean size and particle size distribution) can subsequently be used to predict the age hardening behavior on the basis of the proposed strengthening models [7–10].

The modeling tool has been used to study the precipitation kinetics of aluminum alloys, magnesium alloys and nickel-based superalloys [11–13]. For all these alloys, one precipitate phase was modeled during the simulation. Simulation of Alloy 718 is more challenging since three precipitate phases, γ'' , γ' , and δ , must be considered during the precipitation processes. In this paper, we will study this alloy from both thermodynamic and kinetic points of view. Since the beginning of precipitation depends on the initial state of the material, we will assume uniform elemental distribution and carbides will not be considered in the simulation. In the following, we will first understand the effect of alloying elements on the thermodynamics and phase equilibrium of Alloy 718; we will then perform virtual experiments using this simulation tool to comprehend the co-precipitation behavior of Alloy 718 under various heat treatment conditions.

Thermodynamic Calculation of Composition Effects

The chemistry of Alloy 718 found in literatures varies in a wide composition range. The specification listed in ASM Specialty Handbook for Nickel, Cobalt and Their Alloys [14] is (50–55) Ni; (17–21) Cr; (4.75–5.5) Nb; (2.8–3.3) Mo; (0.65–1.15) Ti; (0.2–0.8) Al; 1.0 max Co; 0.08 max C; 0.35 max Mn; 0.35 max Si; 0.015 P; 0.015 S; 0.006 max B; 0.3 max Cu; and Fe is the balance. To simplify the discussion in the paper, we will ignore the trace elements. The composition ranges for the major elements of Alloy 718 are given in Table 1.

The microstructure of Superalloy 718 is featured by the γ matrix precipitated with ordered DO_{22} γ'' , ordered L1_2 γ' , and δ phase with orthorhombic crystal

Table 1 The composition ranges for the major elements of Alloy 718

	Ni	Cr	Nb	Mo	Ti	Al	Fe
Range (wt%)	50–55	17–21	4.75–5.5	2.8–3.3	0.65–1.15	0.2–0.8	Bal
Medium (wt%)	52.5	19	5.125	3.05	0.9	0.5	18.925

structure. The strengthening mechanism of Superalloy 718 is unique due to the co-precipitation of γ'' and γ' . The γ phase is disordered FCC structure, and it is mainly composed of Ni, Fe, and Cr. The constitution of γ'' and δ can both be described by $\text{Ni}_{0.75}(\text{Nb}, \text{Ti}, \text{Fe}, \text{Cr}, \text{Al})_{0.25}$, with Nb being the major component in the second sublattice. It should be noted that γ'' is a metastable phase which coarsens and transforms to δ phase when exposed at high temperature for long time. The γ' can be described as $\text{Ni}_{0.75}(\text{Al}, \text{Nb}, \text{Ti})_{0.25}$, with Al being the major component in the second sublattice. As is seen, all these three phases compete for the similar elements; the fraction of each phase in the final microstructure therefore depends strongly on the nominal composition and prior thermal-mechanical processing (TMP). In this study, high throughput calculation (HTC) is performed for numerous alloy compositions to view the effects of Al and Nb on the equilibrium fractions of γ'' and γ' at 720 and 620 °C assuming equilibrium is reached at these temperatures. In such a calculation, Al varies between 0.2–0.8 wt%, Nb varies between 4.75–5.5 wt%, Ni is the balance, and all the other components stay at their medium compositions as listed in Table 1. The calculated results are presented as color maps as shown in Fig. 1. It is seen from Fig. 1a, b that the fraction of γ' increases with the increase of Al content in the alloy, while its dependence on the Nb content is not significant. On the other hand, higher fraction of γ'' is obtained when the alloy contains higher Nb but lower Al as is seen in Fig. 1c, d. The negative effect of Al on the fraction of γ'' is due to the fact that higher Al promotes the formation of more γ' which takes away Nb and Ti needed to form γ'' . What we learn from the color maps in Fig. 1 is that Al content must be well optimized and controlled in Alloy 718 to obtain balanced amounts of γ' and γ'' . Higher Al content tends to reduce the fraction of γ'' which is the major strengthening phase of Alloy 718; while lower Al content will eliminate the formation of γ' . In fact, if less than 0.3 wt% of Al is used in the alloy, no γ' will be formed at 720 °C as shown in Fig. 1a.

While the δ -solvus temperature is important in the selection of solution treatment temperature, the reported δ -solvus [15–19] varies between 970 and 1030 °C for cast and wrought Alloy 718. One may find it difficult to understand the big difference; it can be easily justified by Fig. 2. The δ -solvus temperature can indeed vary in a large temperature range depending on the composition of the alloy. Higher Nb and lower Al lead to the formation of δ at higher temperature. The γ'' -solvus temperature follows the same trend. The effect of Ti on the δ -solvus temperature is less significant compare to those of Al and Nb.

The results shows in Figs. 1 and 2 are calculated by using PandatTM software [20] and PanNi2017 database [21]. Although the calculated results were not and could not be validated in the entire composition space shown in these figures, they predict the correct trend and are consistent with experimental observations. Because of the significant effects of alloy composition, small variation on the contents of Al, Nb, and Ti may lead to fairly large difference in the experimental results. It is important to recognize this composition effect when explaining the discrepancies observed from different experimental work. Unfortunately, many published work only give the alloy name, such as Alloy 718, instead of the exact alloy composition.

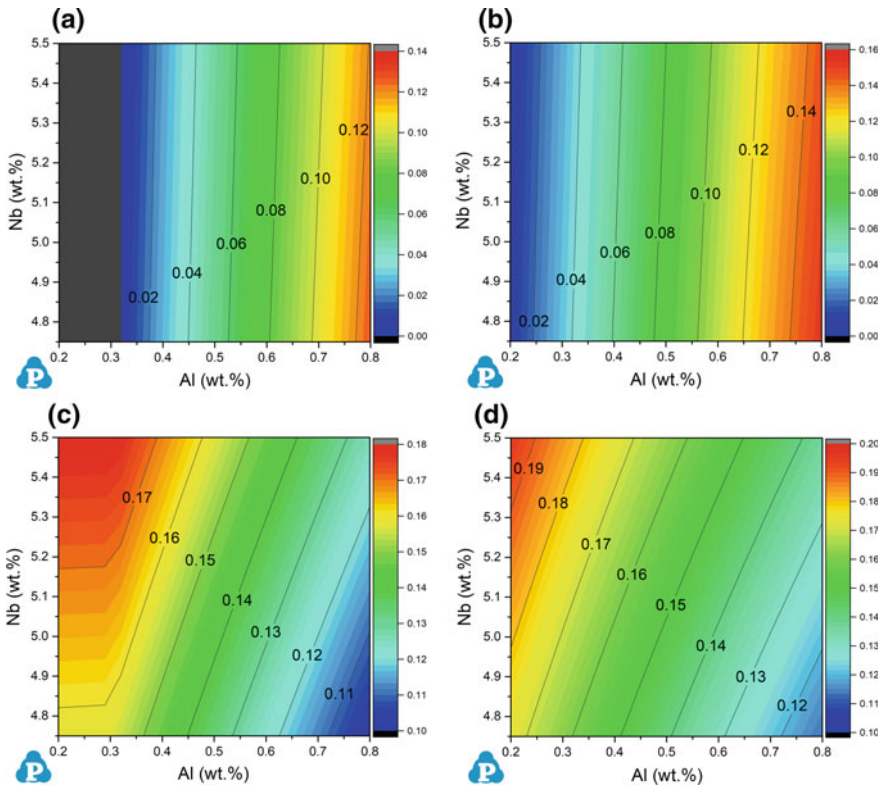


Fig. 1 a, b Equilibrium fraction of γ' at a 720 °C, b 620 °C with varying Al and Nb (Ni balance) c, d equilibrium fraction of γ'' at c 720 °C, d 620 °C with varying Al and Nb (Ni balance)

Precipitation Simulation at Various Heat Treatment Conditions

As mentioned in the introduction section of this paper, although Alloy 718 has been studied for more than 50 years and many data on the processing-property relationship have been collected, systematic study on the co-precipitation kinetics of γ'' and γ' under various heat treatment conditions is very limited. Only a few researchers [22, 23] measured and published particle sizes of γ'' and γ' for Alloy 718 under isothermal ageing conditions. As shown in Fig. 3a, b, simulated particle sizes of γ' and γ'' are compared with the experimentally measured data [22] at two isothermal ageing temperatures, and excellent agreement is obtained. A major adjustable parameter in the precipitation simulation is the interfacial energy. In this calculation the interfacial energies used are 25 mJ/m² for γ/γ' , and 55 mJ/m² for γ/γ'' . The composition is the same as given in Han's work [22]. It should be noted that

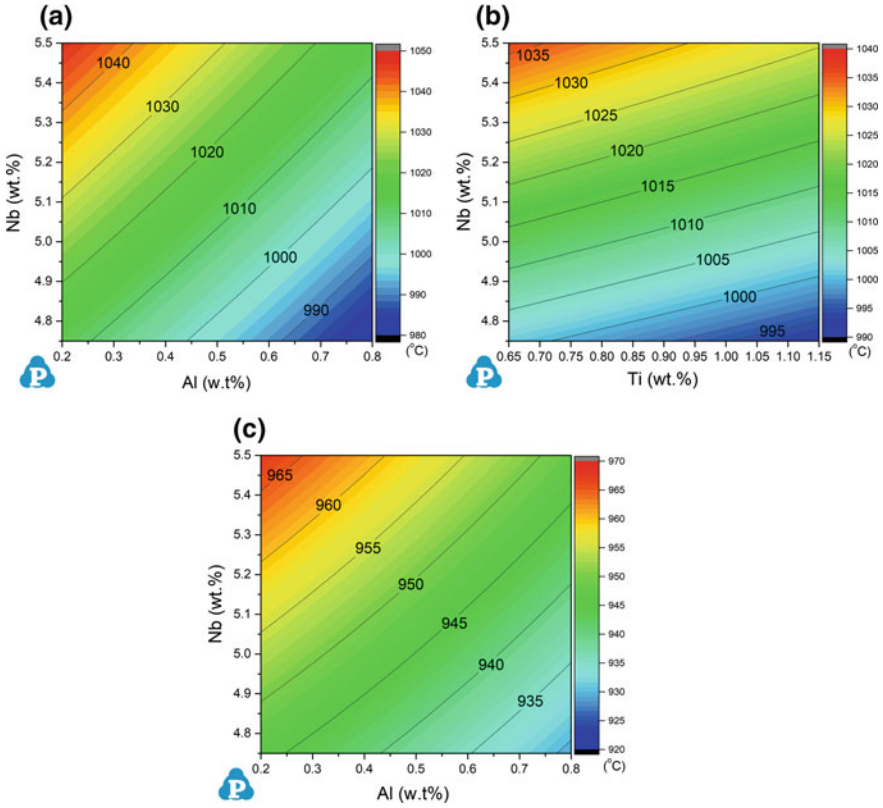


Fig. 2 a, b Solvus temperatures of δ at varying a Al and Nb, b Ti and Nb (Ni as balance) c solvus temperatures of γ' at varying Al and Nb (Ni as balance)

experimentally observed γ' is spherical and γ'' is ellipsoidal [22, 23], while they were both treated as spherical particles in our simulation. The measured size of ellipsoidal γ'' was converted to the radius of a hypothetical sphere by assuming the same volume of the ellipsoid and the sphere, i.e., $V = \frac{1}{6}\pi h(\frac{3}{4}d^2 + \frac{1}{4}h^2) = \frac{4}{3}\pi r^3$ where d is the length of the long-axis, h the length of the short-axis of the ellipsoid, and r the radius of the sphere. Figure 3c is an example micrograph from Han's work [22], which shows spherical γ' and ellipsoidal γ'' .

In this section, we will perform virtual experiments to simulate the effect of various heat treatment conditions on the final microstructure of Alloy 718. As shown in the previous section, the equilibrium fractions of γ' and γ'' , and the δ -solvus and γ' -solvus temperatures depend strongly on the compositions of the alloying elements, especially those of Al, Nb, and Ti. The alloy chemistry, therefore, must be fixed to eliminate the chemistry effect. The medium composition as listed in Table 1 is used in the following calculations. The phase fractions as a function of temperature are calculated for this composition as shown in Fig. 4.

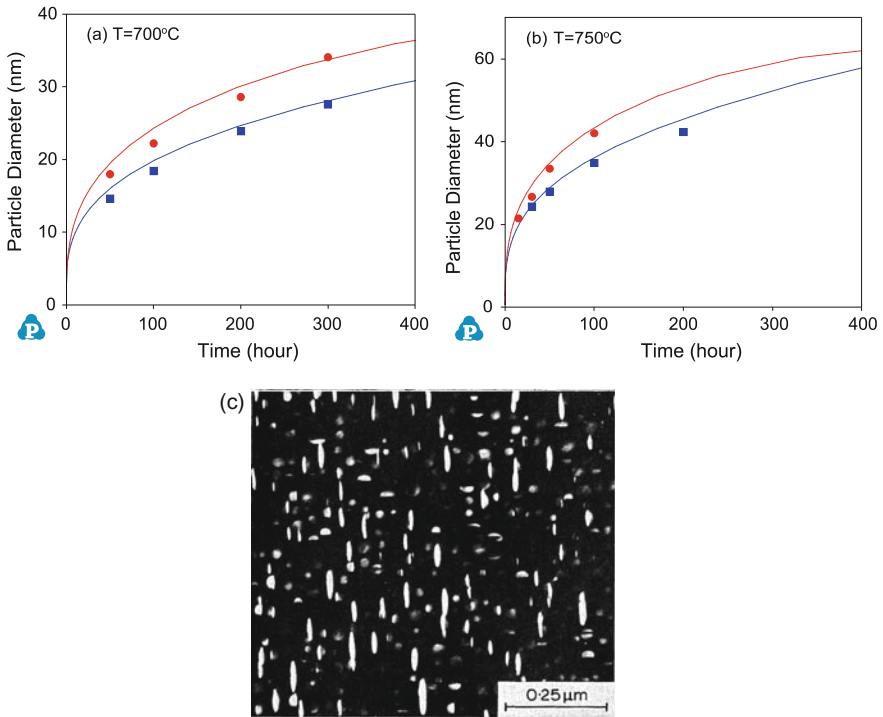


Fig. 3 Evolution of particle sizes of γ' and γ'' at **a** 700°C and **b** 750°C , and **c** an example micrograph from Han's work [22]

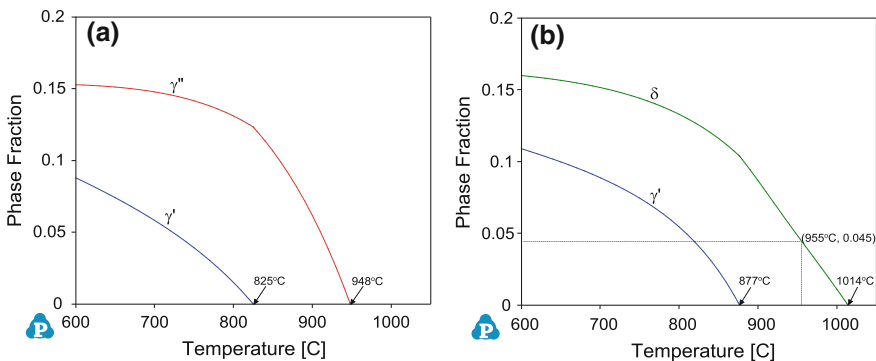
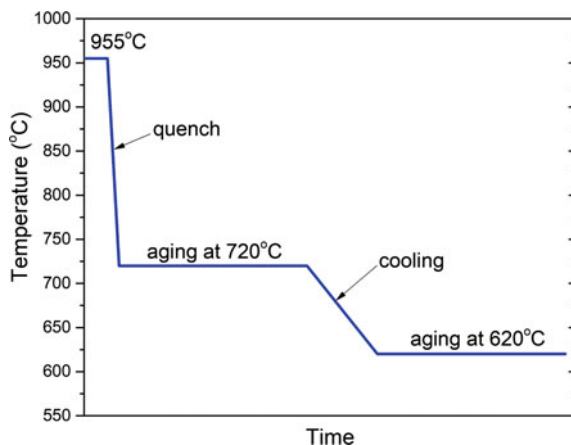


Fig. 4 Calculated fractions of **a** γ' and γ'' , **b** γ' and δ as a function of temperature

The calculated γ'' -solvus and δ -solvus temperatures are 948°C and 1014°C , respectively. It should point out that the δ phase must be suspended when calculating γ'' -solvus since δ is thermodynamically more stable than γ'' . Figure 4a shows

Fig. 5 Simplified heat treatment schedule for Alloy 718 used by this work



the equilibrium between γ' and γ'' , while Fig. 4b is that between γ' and δ . The calculated γ' -solvus temperatures are different for these two cases.

Since the purpose of this study is to understand the competitive precipitation kinetics of γ' and γ'' , the simulation focus is their relative sizes and volume fractions instead of the particle shapes. To simplify the simulation, both of them were treated as spherical particles and the interfacial energies are chosen to be the same as those we used to calculate particle size evolution in Fig. 3.

A typical heat treatment schedule of Alloy 718 usually includes solution treatment at a sub δ -solvus temperature followed by a double-ageing at 720 and 620 °C for 8 h at each temperature. The schedule also includes quenching to room temperature, then heating up to the next step treatment temperature. In this work, this typical schedule is simplified as shown in Fig. 5, i.e., the alloy is solutionized at 955 °C, and then quenched to 720 °C directly for the first stage ageing, then cooled to 620 °C for the second stage ageing. In the following, we will perform simulations based on this simplified heat treatment. We will vary the quenching speed and the length of ageing time to understand the effect of each heat treatment step.

Simplified Typical Heat Treatment Schedule

In this simulation, the simplified typical heat treatment (HT) schedule as shown in Fig. 5 is used. Since the speed of quenching is usually not given in the literature, we assume it takes 0.02 h to drop from 955 to 720 °C, which is equivalent to a speed of 196 °C/min. The speed of cooling between the two ageing temperatures is taken to be 57 °C/h which is the same as mentioned in Bor et al. [24]. paper. The calculated results are shown in Fig. 6. Figure 6a shows the average particle size

evolution of γ' and γ'' . Figure 6b shows volume fraction evolution during the heat treatment process. Logarithm scale is used for time in Fig. 6b to reveal details at early stage. It is seen that γ' precipitated quickly during quenching from 955 to 720 °C due to its coherence with the FCC matrix phase and the small interfacial energy between γ and γ' . However, most of the small γ' particles re-solutionized during ageing at 720 °C. The γ'' particle, on the other hand, grows quickly during ageing at 720 °C. In this simulation, the δ phase is assumed to be in dormant state during the process, i.e., the 4.5% of δ phase obtained during solution treatment at 955 °C (see Fig. 4b) remains unchanged in the microstructure. This point will be further discussed in the later part of this paper. Figure 6c shows particle size distribution at the completion of the heat treatment process. Figure 6d shows volume fraction distribution at the completion of the heat treatment process. In the following, we will vary the speed of quenching and the lengths of ageing time and compare the simulated results with those shown in Fig. 6.

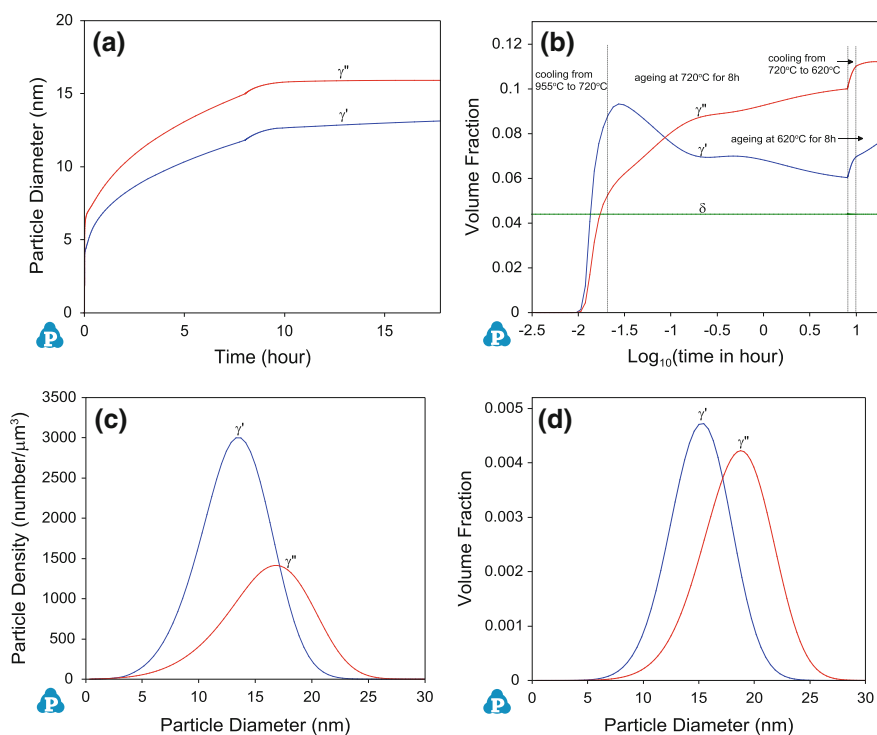


Fig. 6 **a** Average particle size evolution, **b** volume fraction evolution, **c** particle size distribution at the end of HT process, **d** volume fraction distribution at the end of HT process, HT: quenching at 196 °C/min, cooling at 57 °C/h, ageing for 8 h at 720 °C and 620 °C, respectively

Effect of Quenching Speed

In this section, simulation is performed with a slower quenching speed: 39 °C/min, while heat treatment conditions at other stages are kept identical as those used to calculate Fig. 6. The simulated results for the two quenching speeds: 39 °C/min versus 196 °C/min are compared as shown in Fig. 7a–c. As is seen, slower quenching speed allows both γ' and γ'' particles to grow. The γ' phase loses its privilege of fast precipitation during quenching when the alloy is quenched slowly from the solution temperature (955 °C) to the ageing temperature (720 °C). As for the particle size distribution, slower quenching speed leads the distribution curves to bigger sizes with lower densities for both γ' and γ'' particles as shown in Fig. 7c.

Effect of Ageing Time at 720 °C

In this section, simulations are performed to understand the effect of ageing time at 720 °C. Simulations are carried out for a longer ageing time (12 h), and a shorter

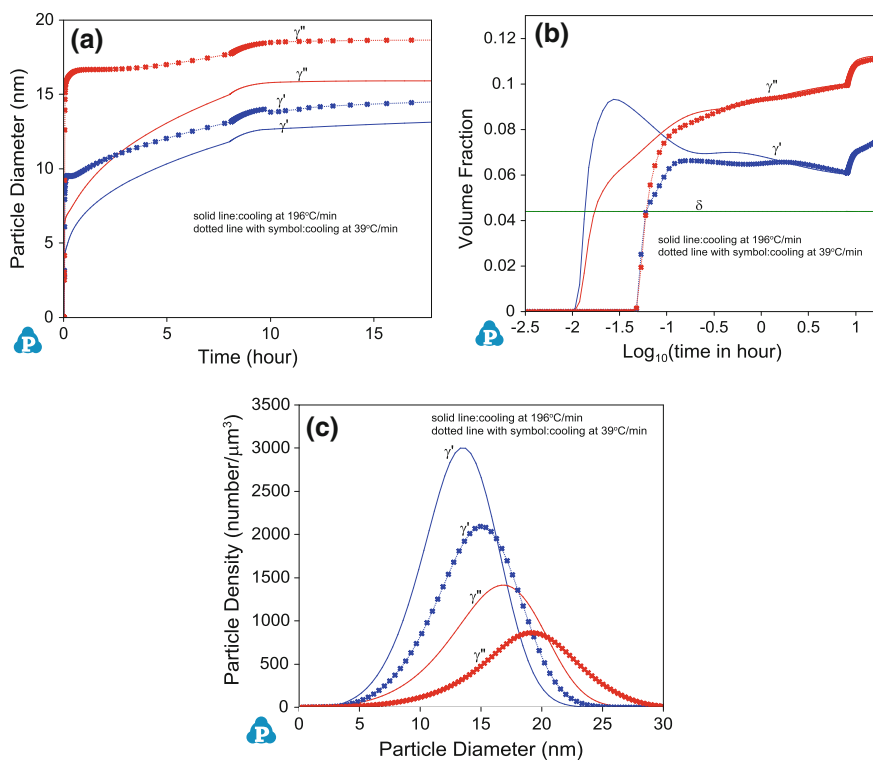


Fig. 7 a Average particle size evolution, b volume fraction evolution, c particle size distribution at the end of HT process, HT: quenching at 196 °C/min versus 39 °C/min, cooling at 57 °C/h, ageing for 8 h at 720 °C and 620 °C, respectively

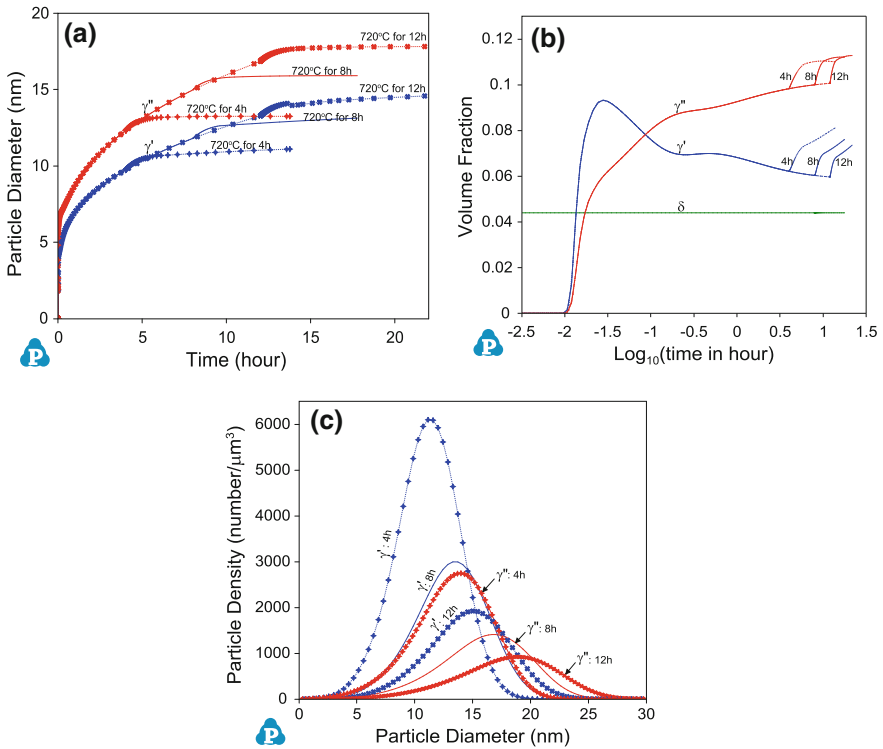


Fig. 8 **a** Average particle size evolution, **b** volume fraction evolution, **c** particle size distribution at the end of HT process, HT: quenching at 196 °C/min, cooling at 57 °C/h, ageing at 720 °C for 8 h versus 4 and 12 h, and ageing at 620 °C for 8 h

ageing time (4 h), and simulated results are compared with those from the typical 8 h ageing as shown in Fig. 8a–c. Clearly, longer ageing hours at 720 °C tends to increase the particle sizes of both γ' and γ'' , while shorter ageing hours has the opposite effect. Shorter ageing time at 720 °C (4 h) leads to slightly higher volume fraction of γ' and lower fraction of γ'' . Regarding the particle size distribution, longer ageing time at 720 °C tends to decrease the number densities and increase the sizes of both γ' and γ'' particles at the end of the heat treatment process as shown in Fig. 8c.

Effect of Ageing Time at 620 °C

In this section, simulation is performed for a longer ageing time (50 h) at 620 °C to understand the effect of ageing time at this temperature. The simulated results are compared with those from the typical 8 h ageing as shown in Fig. 9a–c. Clearly,

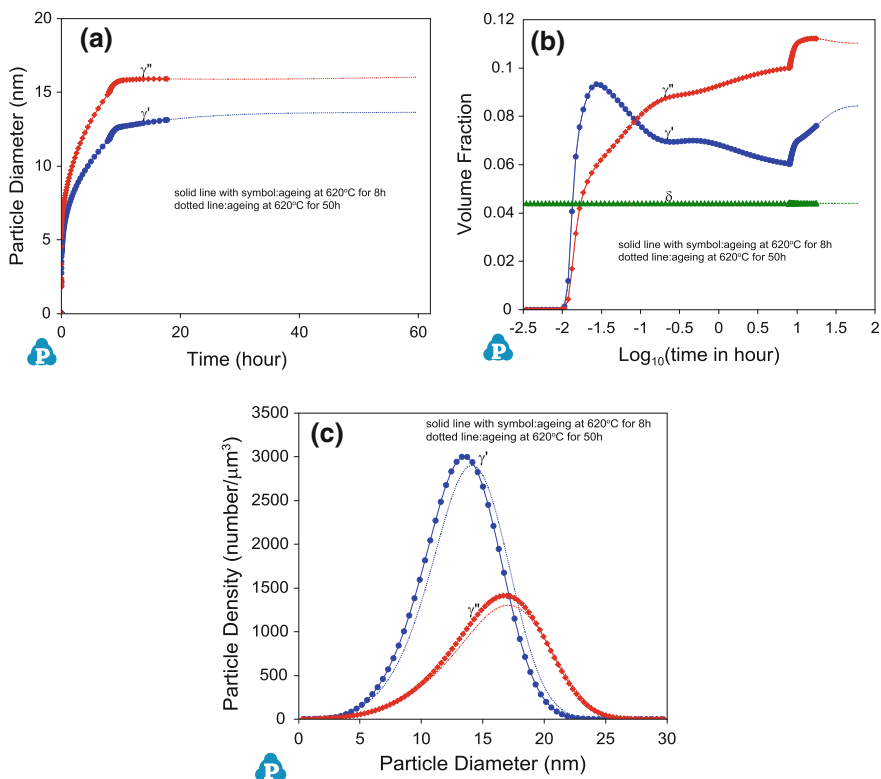


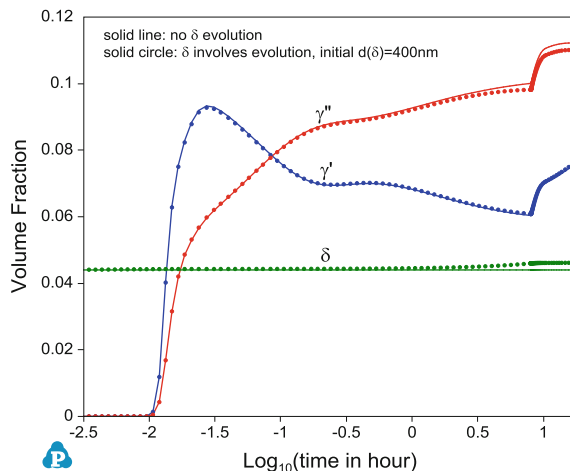
Fig. 9 **a** Average particle size evolution, **b** volume fraction evolution, **c** particle size distribution at the end of HT process, HT: quenching at 196 °C/min, cooling at 57 °C/h, ageing at 720 °C for 8 h, and ageing at 620 °C for 8 versus 50 h

longer ageing hours at 620 °C tends to increase the volume fraction of γ' and decrease the volume fraction of γ'' . Longer ageing hours at 620 °C increases the γ' size slowly, yet it has negligible effect on the size of γ'' .

Effect of δ Evolution

All above simulations focused on the competitive evolution of γ' and γ'' precipitates during the various heat treatment processes, while δ is assumed to be dormant in the microstructure after solution treatment. In other words, the 4.5% of δ phase obtained due to the solution treatment at 955 °C is assumed to keep the same volume fraction and size during the heat treatments. This assumption is valid if the δ particles are relatively large and the interfacial energy between δ particle and γ matrix is high. To view the effect of δ evolution, a simulation considering

Fig. 10 Effect of δ evolution on the evolution of γ' and γ''



competitive evolution of all three precipitates is performed for the same typical heat treatment condition as we used to calculate Fig. 6. The simulated evolution of volume fractions of the three precipitates is shown in Fig. 10. The solid lines represent the case of dormant δ phase, while the solid circles represent the case of active δ evolution. In this simulation, the δ particles in the initial microstructure are assumed to have an equivalent diameter of 400 nm. As is seen from Fig. 10, the volume fraction of δ increases slightly at the consumption of γ'' . The average sizes and size distributions of γ' and γ'' are not plotted since they are almost identical as shown in Fig. 6a, c. Since the needle shaped δ particles obtained after forging and solution treatment usually have an equivalent diameter as large as 500–600 nm, it is believed that their evolution is minimal and their effect on the evolution of γ' and γ'' is negligible during the heat treatment process.

Summary and Conclusion

The co-precipitation kinetics of γ' and γ'' phases in Superalloy 718 was studied in this work using the simulation tool we have developed using the CALPHAD approach. Given a spec range, the composition was found to have significant effects on the thermodynamic properties of Alloy 718, such as the equilibrium volume fractions of the γ' and γ'' phases, and the δ -solvus and γ'' -solvus temperatures. Virtual experiments were performed using the modeling tool to simulate the co-precipitation of γ' and γ'' phases under various heat treatment conditions. Simulation results, such as temporal evolution of volume fraction, number density, and mean size of the precipitates, as well as the final particle size distribution were presented and discussed. The following conclusions are obtained:

- the quenching speed from solution treatment to first step ageing has significant effect on the final particle sizes of γ' and γ'' , not their volume fractions;
- the length of ageing time at 720 °C has significant effect on the final particle sizes of γ' and γ'' , minor effect on their volume fractions;
- the longer ageing time at 620 °C has negligible effect on the final particle sizes of γ' and γ'' , minor effect on their volume fractions;

These virtual experimental results can be used to understand the microstructure observed in Superalloy 718 and may also serve as guidance for further optimization of heat treatment schedule.

References

1. Kaufman L, Bernstein H (1970) Computer calculation of phase diagrams. Academic Press, New York
2. Saunders N, Miodownik AP (1998) CALPHAD-calculation of phase diagrams, a comprehensive guide. Pergamon Press, New York
3. Morral JE, Purdy GR (1994) *Scr Metall Mater* 30:905
4. Lifshitz IM, Slyozov VV (1961) *J Phys Chem Solids* 15:35
5. Wagner C (1961) *Z Elektrochem* 65:581
6. Kampmann R, Wagner R (1984) Kinetics of precipitation in metastable binary alloys—theory and application to Cu-1.9at%Ti and Ni-14at%Al. In: Haasen P (ed) *Decomposition of alloys: the early stages* 1984. Pergamon Press, Oxford, pp 91–103
7. Friedel J (1964) *Dislocations*. Pergamon, Oxford
8. Deschamps A, Brechet Y (1998) *Acta Mater* 47(1):293
9. Myhr OR, Grong O, Andersen SJ (2001) *Acta Mater* 49(1):65
10. Gerold V (1979) *Precipitation hardening*. In: *Dislocations in solids* 1979. North Holland, Amsterdam
11. Cao WS, Zhang F, Chen SL, Zhang C, Chang YA (2011) *JOM* 63(7):29–34
12. Zhang C, Cao WS, Chen SL, Zhu J, Zhang F, Luo AA, Schmid-Fetzer R (2014) *JOM* 66(3):389–396
13. Cao WS, Zhang F, Chen SL, Zhang C, Zhu J, Semiatin SL, Tiley JS (2016) *J Phase Equilib Diffus* 37(4):491–502
14. Davis JR (ed) *ASM specialty handbook: nickel, cobalt, and their alloys*. ASM International
15. Schafrik RE, Ward DD, Groh JR (2001). In: Loria EA (ed) *Superalloys 718, 625, and various derivatives* 2001. TMS, p 1–11
16. Raymond EL (1989). In: Loria EA (ed) *Superalloys 718, 625, and various derivatives* 1989. TMS, p 577–587
17. Groh JR, Radavich JF (1991). In: Loria EA (ed) *Superalloys 718, 625, and various derivatives* 1991. TMS, p 351–361
18. Cao WD (2005). In: Loria EA (ed) *Superalloys 718, 625, and various derivatives* 2005. TMS, p 165–177
19. Stockinger M, Kozeschnik E, Buchmayr B, Horvash W (2001). In: Loria EA (ed) *Superalloys 718, 625, and various derivatives* 2001. TMS, p 141–148
20. Cao W, Chen SL, Zhang F, Wu K, Yang Y, Chang YA, Schmid-Fetzer R, Oates WA (2009) *Calphad* 33:328–342
21. PanNi_TH + MB (2017), Thermodynamic and mobility database for multi-component titanium alloys. CompuTherm, LLC: Middleton, WI 53562, USA. www.computherm.com
22. Han YF, Deb P, Chaturvedi MC (1982) *Met Sci* 16:555

23. He JH et al (1994). *J Mater Sci Technol* 10:293–303
24. Bor HY, Wei CN, Nguyen HT, Yeh AC, Kuo CM, In: Ott EA (ed) *Superalloys 718, 625, and various derivatives 2010*. TMS, p 679–688